AD-A183 026 EFFECT OF PHYSICAL AND GEOMETRIC FACTORS ON THE IMPEDANCE OF ELECTROCHEMI..(U) CASE WESTERN RESERVE UNIV CLEVELAND OHIO DEPT OF PHYSICS B D CAHAN ET AL. 01 MAY 87 TR-1 N00014-86-C-0808 1/1

UNCLASSIFIED F/G 10/2 NL

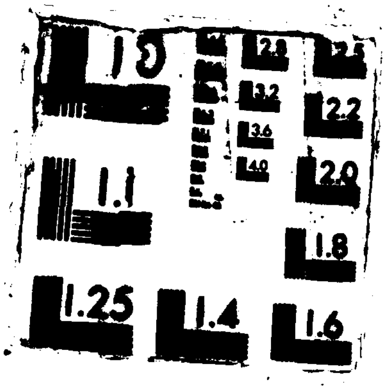
1.0
2.8
2.5
3.2
2.2
3.6
4.0
2.0
1.1
1.8
1.25
1.4
1.6

OFFICE OF NAVAL RESEARCH

Contract N-00014-86-C-0808

Technical Report No. 1

EFFECT OF PHYSICAL AND GEOMETRIC FACTORS ON THE IMPEDANCE OF ELECTROCHEMICAL POWER SOURCES

by

B. D. Cahan, M. L. Daroux and E. B. Yeager

Prepared for Publication

in the

Journal of the Electrochemical Society

Case Western Reserve University
Case Center for Electrochemical Sciences
and the Chemistry Department
Cleveland, Ohio 44106-2699

1 May, 1987

UNCLASSIFIED

SECURITY CLASSIFICATION OF THIS PAGE

AD-A183026

REPORT DOCUMENTATION PAGE

1a. REPORT SECURITY CLASSIFICATION Unclassified	1b. RESTRICTIVE MARKINGS
2a. SECURITY CLASSIFICATION AUTHORITY 2b. DECLASSIFICATION / DOWNGRADING SCHEDULE	3. DISTRIBUTION / AVAILABILITY OF REPORT Approved for public release; distribution unlimited.
4. PERFORMING ORGANIZATION REPORT NUMBER(S) Technical Report No. 1	5. MONITORING ORGANIZATION REPORT NUMBER(S)
6a. NAME OF PERFORMING ORGANIZATION Dept. of Chemistry and Case Center for Electrochemical Sciences 6b. OFFICE SYMBOL *(If applicable)*	7a. NAME OF MONITORING ORGANIZATION Office of Naval Research, Chemistry Code 472
6c. ADDRESS *(City, State, and ZIP Code)* Case Western Reserve University Cleveland, Ohio 44106-2699	7b. ADDRESS *(City, State, and ZIP Code)* Chemistry Progam 800 N. Quincy Street Arlington, VA 22217
8a. NAME OF FUNDING / SPONSORING ORGANIZATION Office of Naval Research 8b. OFFICE SYMBOL *(If applicable)*	9. PROCUREMENT INSTRUMENT IDENTIFICATION NUMBER Contract No. N00014-86-C-0808
8c. ADDRESS *(City, State, and ZIP Code)*	10. SOURCE OF FUNDING NUMBERS PROGRAM ELEMENT NO. | PROJECT NO. | TASK NO. | WORK UNIT ACCESSION NO

11. TITLE *(Include Security Classification)*

EFFECT OF PHYSICAL AND GEOMETRIC FACTORS ON THE IMPEDANCE OF ELECTROCHEMICAL POWER SOURCES

12. PERSONAL AUTHOR(S)

B. D. Cahan, M. L. Daroux and E. B. Yeager

13a. TYPE OF REPORT	13b. TIME COVERED	14. DATE OF REPORT *(Year, Month, Day)*	15. PAGE COUNT
Interim Technical	FROM ______ TO ______	87/5/1	14

16. SUPPLEMENTARY NOTATION

Submitted to the Journal of The Electrochemical Society

17. COSATI CODES			18. SUBJECT TERMS *(Continue on reverse if necessary and identify by block number)*
FIELD	GROUP	SUB-GROUP	Impedance of Electrochemical Power Sources, Computer Modeling of Electrochemical Cells, Pulsed High Power Batteries

19. ABSTRACT *(Continue on reverse if necessary and identify by block number)*

Short-time transient behavior in the charge/discharge of small electrochemical power sources does not scale up for large systems. Calculations are presented which show that a number of commonly neglected physical and geometric factors, such as the skin effect and the distributed network impedance characteristics of the individual cells and cell assemblies, can severely limit performance. The impedance of individual cells has been calculated over a wide range of frequencies (10^2-10^8 Hz) using a modified semi-infinite strip-line model. The variables considered include the electrode and electrolyte conductivities, the electrolyte dielectric constant, the double-layer capacitance, and the distributed inductance and capacitance resulting from the cell geometry.

100 - 10 to the 8th

(Keywords

20. DISTRIBUTION / AVAILABILITY OF ABSTRACT ☐ UNCLASSIFIED/UNLIMITED ☒ SAME AS RPT ☐ DTIC USERS	21. ABSTRACT SECURITY CLASSIFICATION Unclassified
22a. NAME OF RESPONSIBLE INDIVIDUAL Dr. Robert Nowak	22b. TELEPHONE *(Include Area Code)* (202) 696-5075 | 22c. OFFICE SYMBOL

EFFECT OF PHYSICAL AND GEOMETRIC FACTORS ON THE IMPEDANCE OF ELECTROCHEMICAL POWER SOURCES

B. D. Cahan, M. L. Daroux and E. B. Yeager

The Chemistry Department and the Case Center
for Electrochemical Sciences,
Case Western Reserve University,
Cleveland, Ohio, 44106

INTRODUCTION:

Only a relatively small amount of work has been published [1-3] on the transient response of high power battery systems in the short time domain (0.1μs-10ms). Most laboratory studies deal with scaled down versions of large cells that are in practice usually employed to provide standby power or for applications in which continuous operation is required, rather than for pulse generation. In the present work, the impedance of an individual elementary cell has been calculated over a wide range of frequencies in order to show the effects of various physical and geometric factors that are significant at short discharge times.

The geometry chosen for the present calculations is the semi-infinite parallel plate cell with infinitely thick solid electrodes; a configuration commonly referred to in the electronics literature as a strip-line. Such a cell is illustrated schematically in Fig. 1. In order to carry out the impedance calculation this battery cell has been modelled as a transmission line containing uniformly distributed values of resistance, capacitance and inductance; quantities that can be determined directly from the physical characteristics chosen for the model. The transmission line can be analysed as a distributed network of differential elements [4], each having the equivalent circuit shown in Fig. 2. Its electrical characteristics can then be expressed in terms of a characteristic impedance Z_o, an attenuation constant α, and a phase shift β.

$$Z_o = \left(\frac{r_s + j\omega L_s}{g_p + j\omega C_p}\right)^{1/2} \qquad ....(1)$$

where r_s is the series resistance, g_p is the shunt conductance, L_s is the series inductance, and C_p is the shunt capacitance, all per unit length.

The propagation constant γ for the transmission line shown in Fig. 2 is given by the expression

$$\gamma = [\,(r_s + j\omega L_s)\cdot(g_p + j\omega C_p)\,]^{1/2} \qquad ....(2)$$

The propagation constant can also be written in terms of its real and imaginary parts, as

$$\gamma = \alpha + j\beta \qquad ....(3)$$

The real part, α, is the attenuation constant and is related to the penetration length of the perturbation (along the z axis in Figure 1). β is the phase constant. The attentuation constant is given by the expression

$$\alpha = r_s/2Z_o + g_p Z_o/2 \qquad ....(4)$$

For a particular frequency all but 1/e of the total current is drawn from a distance $1/\alpha$ from the terminals. This distance is referred to as the penetration length. The ratio of currents between points O and X, separated by a distance x, for a wave going from O to X, is

$$I_x / I_o = e^{-\alpha x} \qquad ....(5)$$

In the corresponding time domain, this implies that at short times almost all the current is generated within about one penetration length (i.e., in the regions closest to the current collection terminals). Regions further along the z axis in Fig. 1 make little or no contribution. The utilization increases with time, but for short times a cell need have a length of only on the order of 2 or 3 times the penetration length in order to show the behaviour of a semi-inifite cell.

The above treatment yields the impedance as a function of frequency, but what is preferred in practice is the current/voltage response as a function of time when a cell or battery is placed on load. In principle it should be possible to compute the transient response by multiplying the impedance function by the transform of the perturbation and carrying out an inverse transformation on the product. This will be the subject of a future paper.

ESTIMATION OF PARAMETERS

There are four parameters, r_s, g_p, L_s and C_p in the lumped network representation of a unit section of transmission line shown in Fig. 1. The physical components of such a cell are illustrated schematically in Fig. 1, and the corresponding equivalent circuit is given in Fig. 3. In order to calculate the impedance, Fig. 3, the equivalent circuit representation of the physical components, must be translated into the form of Fig. 1.

The values of the parameters in Fig. 3 can be obtained from the physical properties chosen for the model as follows: r_s and L_s are modified by the skin effect [5]. The magnetic field resulting from current flow in a cell configured as a transmission line confines the current to the outer layer (skin) of the conductors. This is seen at high frequencies as an exponential decrease in current density in a conductor as the distance away from the surface increases. The equivalent skin depth, d, is defined as that depth over which a current density equal to 0.707 of the surface current density can be considered to be distributed uniformly.

$$d = 1/(\sigma\pi f\mu)^{1/2} \qquad \ldots.(6)$$

where σ is the conductivity in $\Omega^{-1}.m^{-1}$, f is the frequency in Hz, and μ is the permeability in Henries.m^{-1}. Thus, even for an infinitely thick plate, at high frequencies all but 1/e of the current will be carried by a depth d of the outer region.*

The series inductance arises from the geometry of the conductors and is given, when the skin depth d (or the thickness of the electrodes themselves for finite thickness electrodes) is small with respect to the cell width W, by

$$L_s = 1.255\times10^{-6}\cdot u/W \qquad \ldots.(7)$$

where u is the electrode spacing, and L_s has units of Henries/m. The series resistance for the infinitely thick electrodes assumed is dominated by the skin effect resistance r_{sk}, which is given by

$$r_{sk} = 3.974\times10^{-3}\cdot\rho_m^{1/2}\cdot f^{1/2}/W \qquad \ldots.(8)$$

where ρ_m is the resistivity of both electrodes in Ω-m, and r_{sk} has units of Ω/m. In the present model it is assumed that all plates and current collectors are infinitely thick, so r_s is determined solely by r_{sk} which in turn depends on the skin depth and on the conductivity of the electrodes (i.e. the calculations assume the best case). For example, the skin depth for copper at 6×10^5Hz is 0.6mm and the resistance increases above that calculated using equation (7) as the plate thickness approaches and becomes smaller than this value. It should be noted that for electrodes of lower conductivity (because of either intrinsic conductivity or porosity) the skin depth increases in proportion to the square root of the resistivity. In consequence, the effective resistance will only increase in proportion to the square root of an increase in electrode resistivity.

It should be noted that r_{sk} is a function of frequency although by definition a real resistance is frequency invariant, yet the phase angle remains zero. This is in apparent contradiction of the Kramers-Kroenig relations [7], but it must be recognised that r_{sk} is only an effective resistance and is a result of the nonuniform distribution of current density into a conductor at AC frequencies.

The parallel components comprise terms for the electrode interfaces in series with terms for the electrolyte. The interfacial components are represented by the parallel combination of a Faradaic resistance, r_F, and a double-layer capacitance, C_{dl}. The electrolyte terms are the Ohmic resistance, r_E, and in parallel the dielectric capacitance, C_E, where [5]

$$C_E = \epsilon.\epsilon_o.W/u \qquad \ldots.(9)$$

*NOTE: The skin depth is often surprisingly small. Sixty hertz power transmission lines are rarely larger than two skin depths in diameter ($d_{Cu[60Hz]}$ = 6mm). Increasing the diameter of the wire decreases the resistance in proportion to the circumference rather than to the cross-sectional area.[6]

ϵ is the dielectric constant of the electrolyte, and C_E is in units of Farads/m^2. In the model discussed here, the interface is considered to be smooth.

The series impedances for the interfaces and for the electrolyte must then be combined in series and then converted to a complex admittance of the form $g_p + j\omega C_p$ for use in equation (3). It should be noted that g_p and C_p here do not correspond to any simple physical quantities.

RESULTS AND DISCUSSION :

The strip-line cell shown in Fig. 1 has been modelled as a transmission line. The impedance per unit width and length has been computed as a function of frequency for different values of electrode and electrolyte conductivity and cell thickness. For the purposes of these initial calculations, the case where no Faradaic processes are occurring has been considered; that is the Faradaic resistance, r_F in Fig. 3, has been considered to be infinite. A constant, frequency-independent double-layer capacitance of 50uF/cm^2 has been used, and it has been assumed that the electrodes are infinitely thick so that the series resistance is equal to r_{sk}. The cell is assumed to be infinitely long, although only a small fraction of this length will actually be able to deliver current to a load at short times or high frequencies. The penetration length has been calculated as a function of frequency for each set of conditions.

The results are presented as Bode plots for log Z, the logarithm of the modulus of the complex impedance (equivalent to log $|Z_o|$), the phase angle θ, and the penetration length (equal to $1/\alpha$ - equation (5)).

Depending on the values of the physical variables chosen for the calculation, the equivalent circuit shown in Figure 2 can be simplified to yield a number of limiting cases. If ωL_s and ωC_p are small with respect to r_s and g_p, respectively, then the characteristic impedance, Z_o, will be resistive in nature. If ωL_s and ωC_p are large with respect to r_s and g_p, then the circuit will reduce to an LC network and Z_o will again be resistive. If ωC is small with respect to g_p only then the circuit reduces to an RL network and Z_o will show a positive phase shift, while if ωL is small with respect to r_s only then the circuit reduces to an RC network and Z_o has a negative phase shift. The results of the calculations presented here indicate that, depending on the frequency range of interest and the values of the physical variables chosen, a number of these different limiting cases as well as intermediate behaviour will be observed with real cells.

Figure 4 is a set of Bode plots calculated for electrode resistivities ranging from 1.7×10^{-6} to 1.7×10^{-1} Ω.cm. It may be noted that Cu has a resistivity of 1.7×10^{-6} Ω.cm. The cell thickness is 0.01cm, while the electrolyte resistivity has been set high at 1.0×10^{10} Ω.cm. This latter value gives the limiting case where ωC_p is large with respect to g_p. Figure 4 shows that at high frequencies, for the lower values of ρ_M, ωL_s is much greater than the series resistance, r_s, and the behaviour of the cell approaches that of a pure LC strip line. (It can be seen from equation (1) that if $r_s = g_p = 0$, then the $j\omega$ factors cancel and Z_o becomes wholly real.) Z

approaches a constant, purely resistive, value of about 5Ω (determined largely by the values chosen for the cell thickness and the electrolyte dielectric constant), while θ tends to zero.

For more resistive electrodes and at lower frequencies, the contribution from the series resistance term is larger, and the overall behaviour becomes capacitative. The impedance increases, while θ tends to -45°. For Cu, for example, Z begins to increase at a frequency of about 10^6Hz. It might be expected that as r_s becomes dominant at low frequencies (since r_{sk} decreases in proportion to only the square root of f) and/or as the resistivity of the electrode increases, the behaviour of the transmission line would approach that of an RC network. For this case the Kramers-Kroenig relations [4] predict that when θ goes to -45°, log Z should decrease with frequency with a slope of -1/2. However Figure 4 shows that the computed value of log Z only decreases with a slope of -1/4. The probable explanation for this behaviour is that not only the values of the circuit components but also the equivalent circuit representation that is applicable changes with frequency. This result provides a further illustration of the necessity of predicting the time or frequency dependent behaviour of distributed systems from computations based on a complete model, rather than on intuitive extrapolations from steady state behaviour. It is not in general valid to replace a distributed network by a single simple equivalent circuit. In the model used here, r_s continues to change with frequency because an infinite electrode thickness has been assumed. If instead, a finite plate thickness is assumed, then once the skin depth exceeds this thickness (at low frequencies - see equation (8)), r_s should tend to a constant value and the slope of log Z should tend to -1/2.

The penetration lengths are also shown in Fig. 4, and it can be seen that for this case of a highly resistive electrolyte they are relatively large over almost the whole frequency range. At low frequencies they decrease by less than an order of magnitude as the electrode resistivity increases by six orders of magnitude. At the higher frequencies electrode resistivity has almost no effect on the penetration length.*

Figure 5 shows the same calculation as that shown in Figure 4 performed for a cell thickness of 0.1 cm. It can be seen that the resulting set of Bode plots have the same shape, but that the impedance curves have been shifted upwards (to higher impedances), and both the log Z and the θ curves have been translated to the left, i.e. to lower frequencies. The penetration length is increased slightly at lower frequencies. These changes in the limiting behaviour are the result of the order of magnitude decrease in the dielectric capacitance of the cell corresponding to the order of magnitude increase in electrode spacing. Because this quantity is much smaller than the double-layer capacity, it dominates the value of C_p. (See Figure 3.) The limiting value of Z increases because C_p decreases and also because L_s increases with the increase in spacing (equation (1)).

---

* NOTE: The calculation above corresponds to the case of a cell having a highly-resistive (e.g. nonaqueous) electrolyte and indicates that significant currents can still be drawn. The calculation also applies to a capactitor having a configuration corresponding to this strip line, which will also demonstrate resistive behaviour at high frequencies and a significant increase in impedance at low frequencies.

Figure 6 shows the effect of varying the electrolyte resistivity over the range 10^{-2} to 10^{3} Ω.cm when the electrodes are highly conductive. The cell thickness is 0.1 cm, and ρ_M is 1.7×10^{-6} Ω.cm. Over a wide frequency range, from 10^{2} to 10^{8} Hz depending on the value of ρ_E, g_p is much larger than ωC_p and the transmission line shows a positive phase shift. This region is characterised by log Z increasing with increasing frequency with a slope of 1/2, while the phase angle tends to +45°. This is the behaviour expected for an LR stripline. The frequency at which this behavior is seen depends on the value of ρ_E, shifting to lower frequencies as ρ_E increases. At still lower frequencies r_s becomes large with respect to ωL_s, and log Z reaches a constant value (about 0.002 Ω) characteristic of purely resistive behaviour. Correspondingly, θ decreases to zero.

At frequencies above the LR region ωC_p becomes increasingly significant, and as it exceeds g_p the behaviour of the line again becomes resistive (see the discussion of an LC network above). Log Z tends to a new limiting value, almost two orders of magnitude greater, and θ decreases to zero.

Figure 6 also shows that the penetration length is strongly dependent on the electrolyte resistivity, decreasing as ρ_E decreases.

Figure 7 shows the effect of electrolyte resistivity when the electrodes have a relatively low conductivity. Again ρ_E ranges from 10^{-2} to 10^{3} Ω.cm, while the electrode resistivity is 3.5×10^{-3} Ω-cm, corresponding to an electrode material such as carbon. The electrolyte thickness is 0.1 cm.

Over limited frequency ranges, the behavior of the cell can be described by simplified versions of the equivalent circuit shown in Fig. 2, and these are illustrated in Fig. 7 for the curve corresponding to an electrolyte resistivity of 10^{2} Ω-cm. At high frequencies (region E), this transmission line behaves like an LC network and Z_o has the characteristics of a pure resistance (see equation (1)). Log Z is constant, and the phase shift, θ, approaches zero. As the frequency decreases (region D) ωC_p becomes less than g_p and the behavior becomes that of the LR circuit shown. The impedance decreases, and θ becomes positive. As the frequency continues to decrease (region C) ωL_s becomes comparable to r_s and the equivalent circuit tends to become purely resistive as shown (region B). At the lowest frequencies shown (region A) the interfacial terms begin to become important. Here ωC_{dl} starts to become the dominant parallel component and the impedance increases again, while θ becomes negative. This may be a consequence of the assumption of infinitely long plates and infinitely thick electrodes. As the skin depth continues to increase with decreasing frequency, the penetration length may become limiting. It should be noted that the Kramers-Kroenig relationship does not hold here either, since α depends on r_s which is frequency dependent.

As in the previous example the penetration length is dominated, particularly at high frequencies, by ρ_E. The effect of the lower value for ρ_M appears as a slight decrease in the penetration length at low frequencies.

From the examples above, it may be concluded that at high

frequencies/short times the behaviour of the simple cell modelled here is limited by the impedance resulting from the physical geometry of the cell components. These factors must therefore be given strong consideration when designing batteries for high-power short-duration pulse applications. The continuation of this work is now in progress to extend the model to take into account the effects of the electrochemical interface and more complex cell geometries.

SUMMARY :

1. The impedance resulting from the physical geometry of the components will limit the high frequency/short time performance of a cell and must therefore be considered in addition to the electrode kinetics in designing short duration pulse batteries.

2. In order to take these effects into account in estimating battery performance, it is necessary to model the battery as a complex distributed network. The behavior of these networks does not follow intuitive concepts applicable to steady-state behaviour or to systems that can be uniquely represented by a simple equivalent circuit. Depending on the condition chosen, any of the variables considered, i.e., electrode resistance, electrolyte resistance, or cell thickness, can affect the performance of a cell.

3. The calculated values of penetration length indicate that at short times/high frequencies current can only be drawn from the regions closest to the terminals of most conventional large battery cells, so that only a fraction of their total power is available. This problem becomes greater as the size of the battery is increased since the ratio of $1/\alpha$ to cell dimensions becomes increasingly unfavorable. Transients measured for small test cells should not necessarily be expected to scale as the cell/battery size is increased.

ACKNOWLEDGEMENTS: This research has been supported by ONR through a subcontract with Eveready Battery Co. We thank Dr G. Blomgren, Dr J. Bailey and Ms J. Boyd for helpful disscussions.

REFERENCES:

[1] P.L. Kapitza, Proc. Roy. Soc. Lond., 105A, 691, (1924)

[2] J.J. Lander, E.E. Nelson; J. Electrochem. Soc., 107, 722, (1960)

[3] R.M. LaFollette, D.N. Bennion; 171st ECS Meeting Extended Abstracts, 87-1, p40, Abs. #29, Philadelphia, (May,1987) and references therein.

[4] R.W. Landee, D.C. Davis, A.P. Albrecht; "Electronic Designers' Handbook" Chap. 20, McGraw-Hill, N.Y. (1957)

[5] F.W. Sears, "Principles of Physics II.Electricity and Magnetism", Chap.7, Addison-Wesley, Cambridge, Mass. (1947)

[6] P. Grivet, "The Physics of Transmission Lines at High and Very High Frequencies", Vol. 1, Ch. 2, Academic Press, Lond. (1970).

[7] H.W. Bode, "Network Analysis and Feedback Amplifier Design", Van Nostrand, Princeton, (1945)

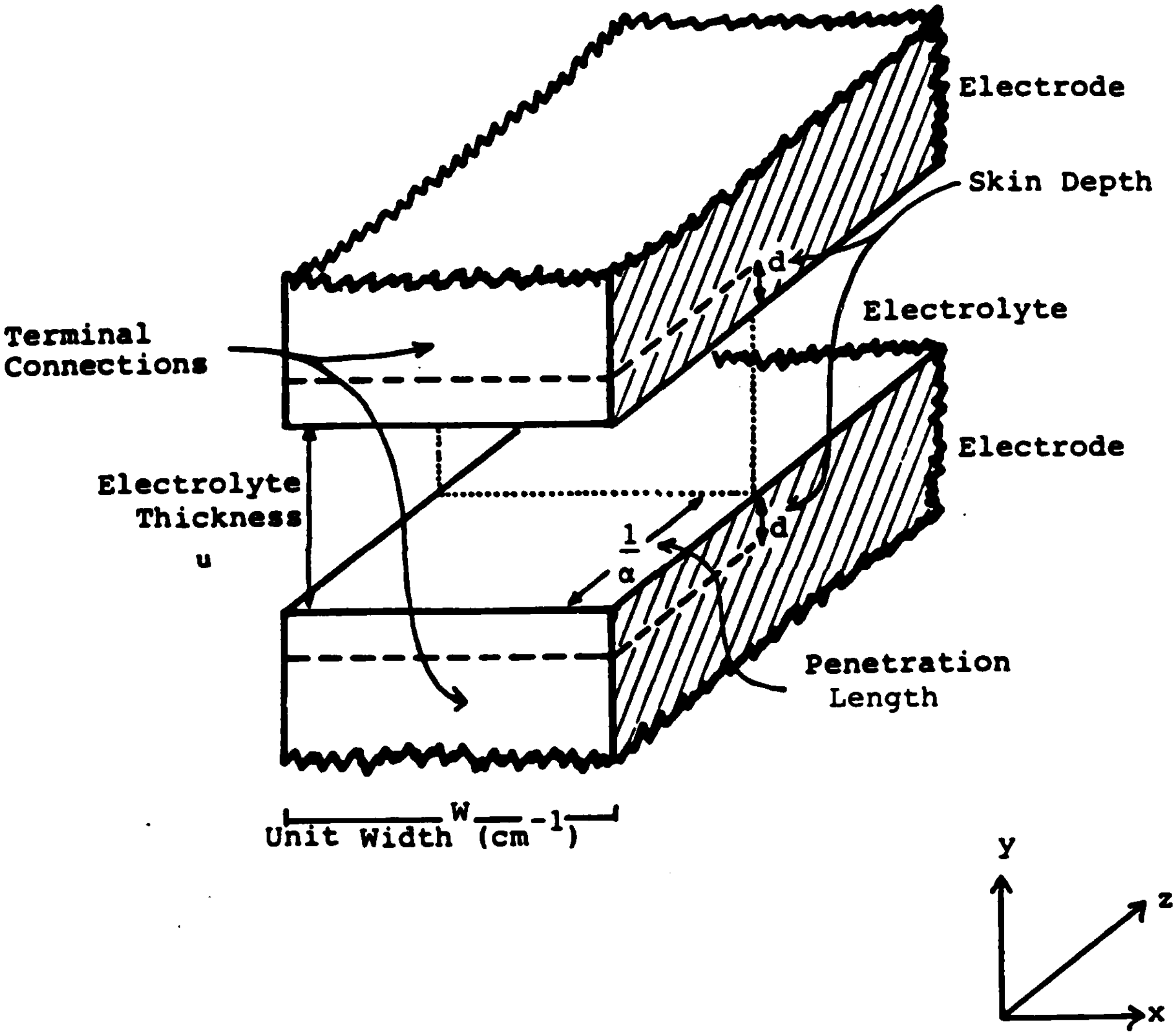

__FIGURE 1__ : Physical Geometry of Semi-infinite Parallel Plate (Strip-line) Cell

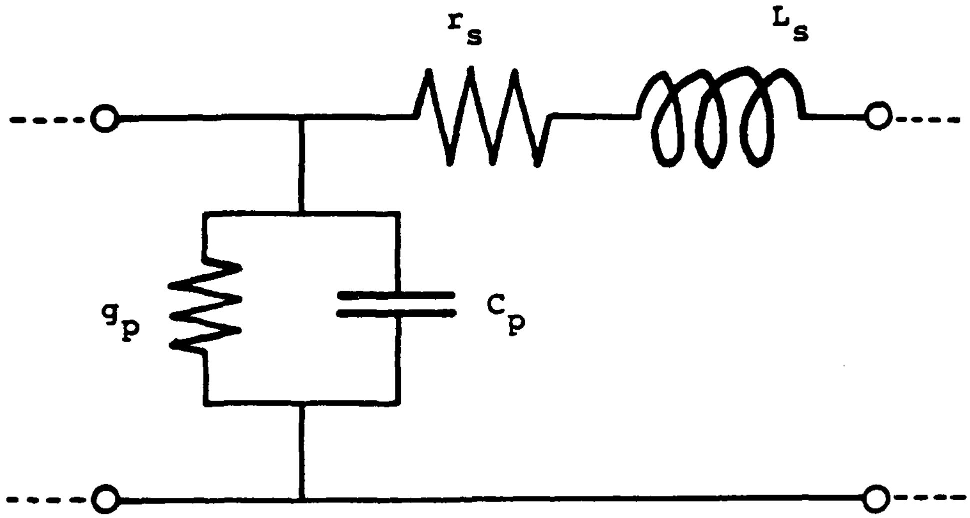

FIGURE 2 : Equivalent Circuit of Individual Element in Distributed Network Analysis of Strip-line Cell

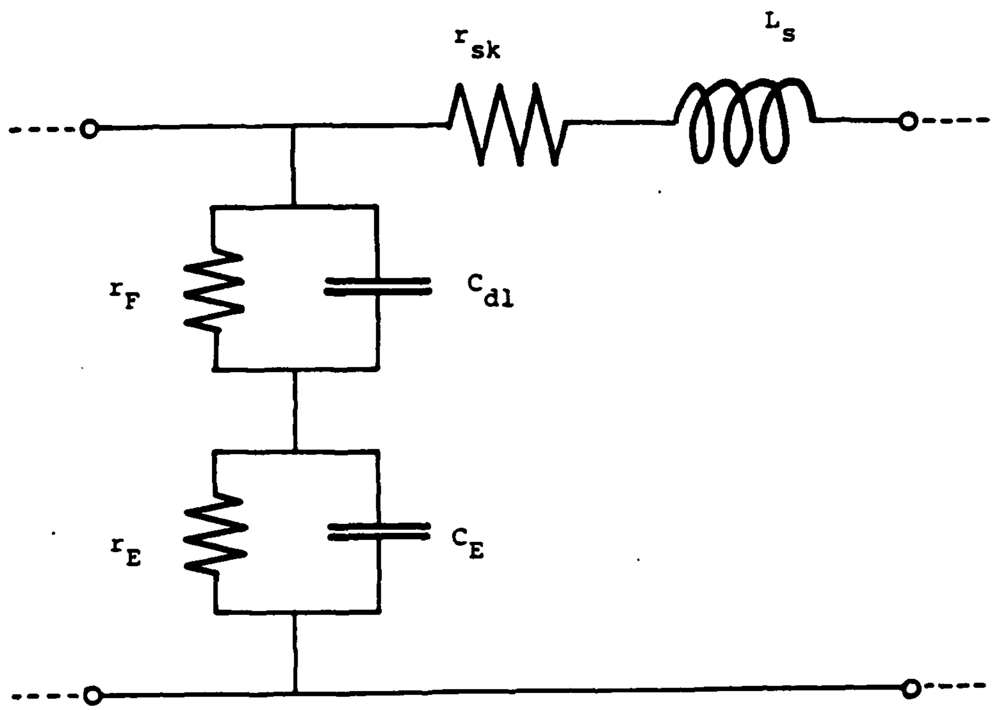

FIGURE 3 : Equivalent Circuit Representation of Physical Components of Strip-line Battery Cell

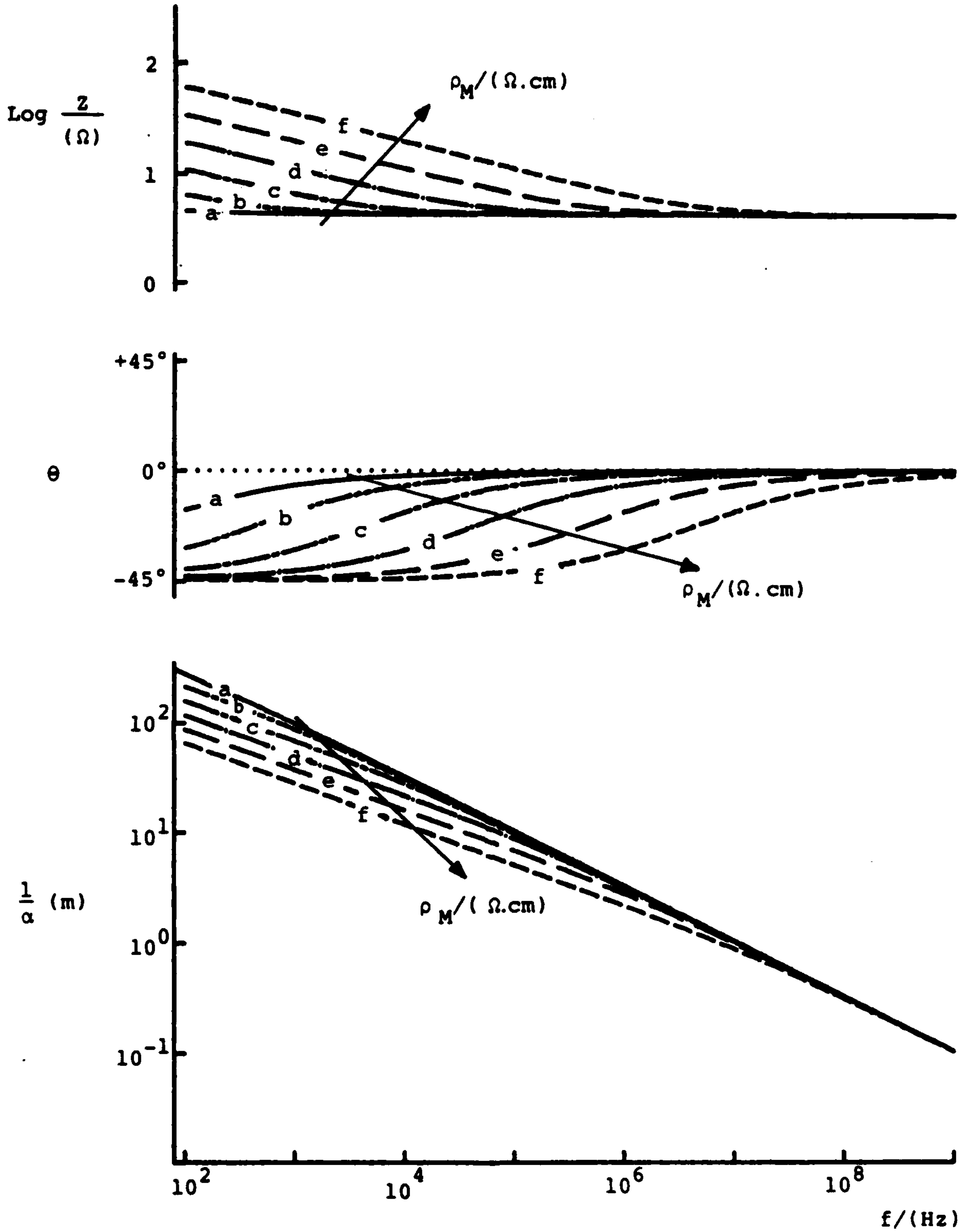

FIGURE 4 : Bode Plots showing a) log Z, b) θ and c) $1/\alpha$ (penetration length), as a Function of Frequency. Calculated for $\rho_m = 1.7\times10^{-6}$(curve (a)) - 1.7×10^{-1}(curve (f)) Ω-cm, u = 0.01 cm, ρ_E(electrolyte resistivity) = 10^{10} Ω-cm, W = 1.0 cm, C_{dl} = 50 uF/cm^2, $C_E = 7.17\times10^{-5}$ μF/cm^2, $L_s = 1.255\times10^{-9}$ H/m.

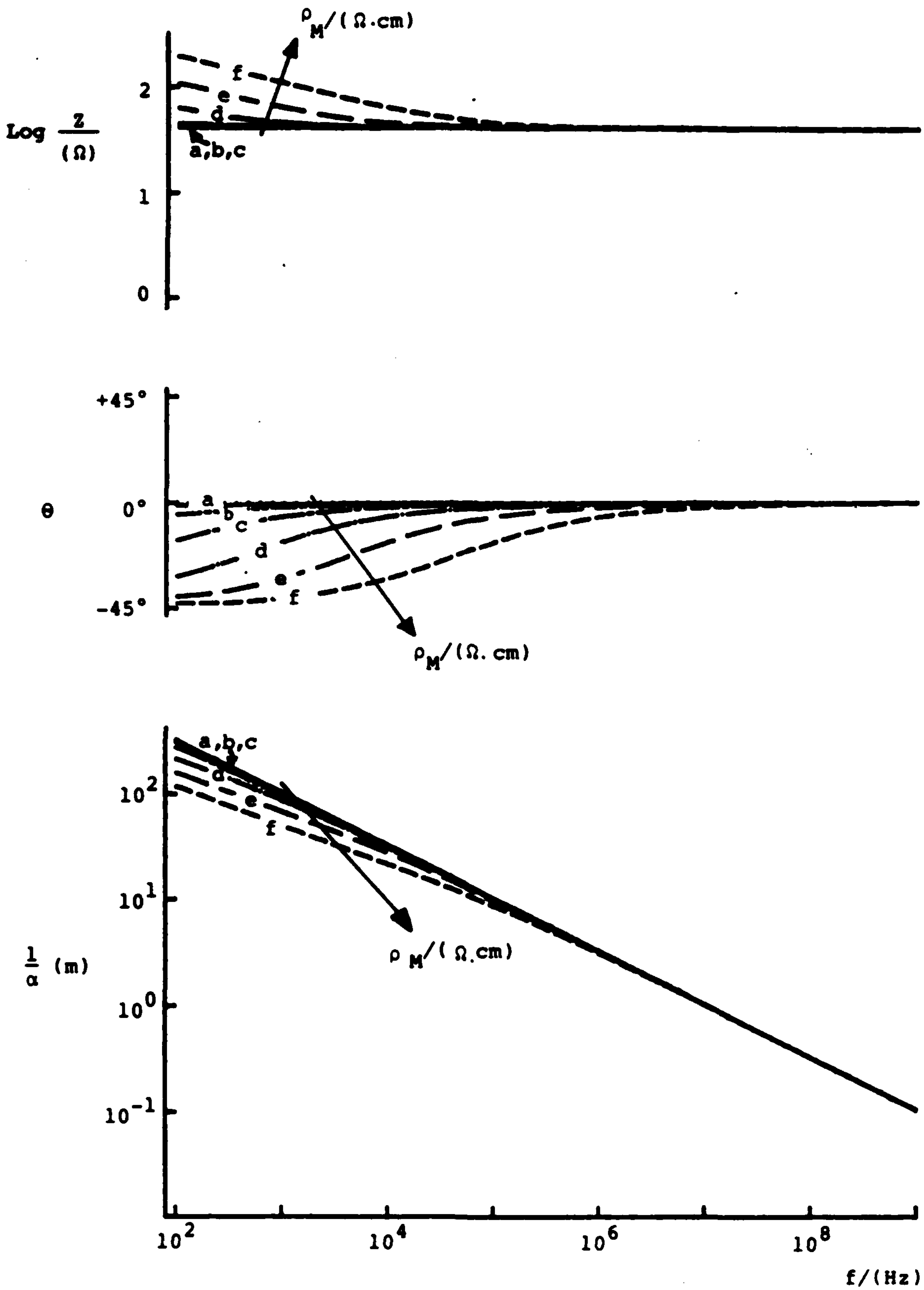

FIGURE 5 : Bode plots for $\rho_E = 10^{10}$ Ω.cm, u = 0.1 cm, W = 1.0 cm, C_{dl} = 50 $\mu F/cm^2$, $C_E = 7.17\times10^{-5}$ $\mu F/cm^2$, $L_g = 1.255\times10^{-9}$ H/m, $\rho_m = 1.7\times10^{-6}$(curve (a)) - 1.7×10^{-1}(curve (f)) Ω-cm.

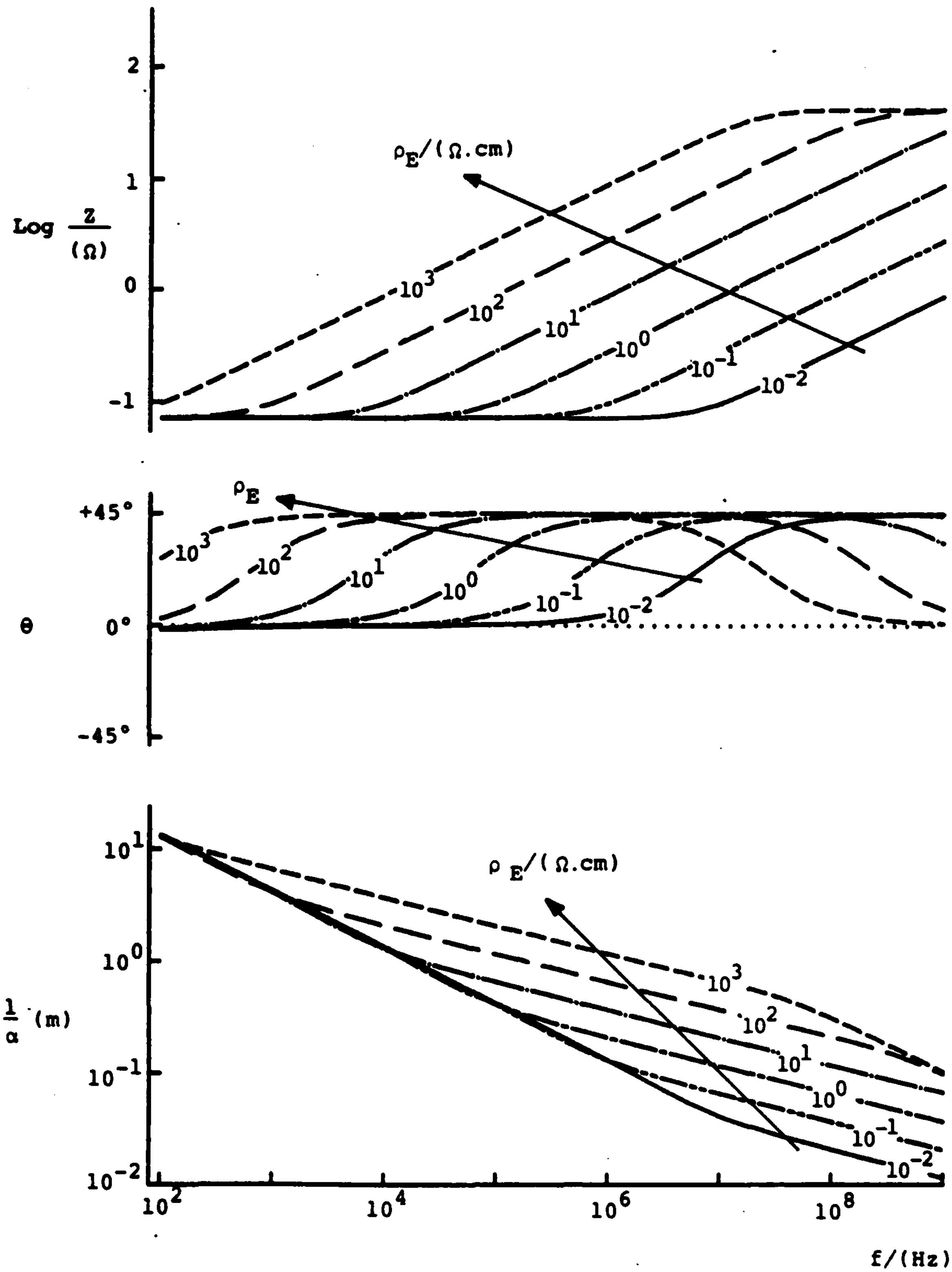

FIGURE 6 : Bode plots for $\rho_m = 1.7\times10^{-6}$ Ω-cm, $\rho_E = 10^{-2} - 10^3$ Ω-cm, u = 0.1cm, W = 1.0 cm, $C_{dl} = 50\ \mu F/cm^2$, $C_E = 7.17\times10^{-5}\ \mu F/cm^2$, $L_s = 1.255\times10^{-9}$ H/m.

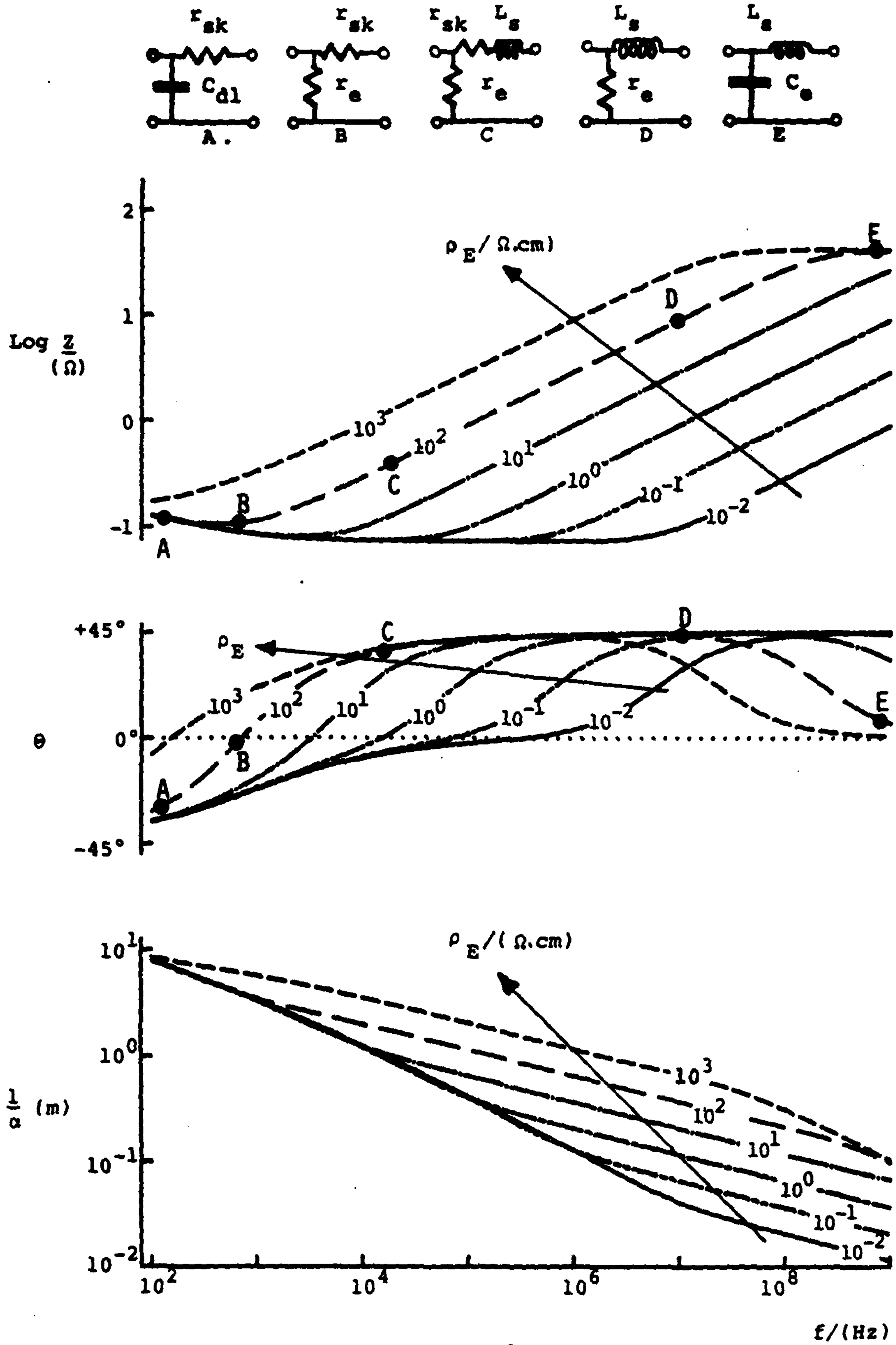

FIGURE 7 : *Bode plots for* ρ_m = 3.5×10^{-3} Ω-cm, ρ_E = 10^{-2} - 10^{3} Ω-cm, u = 0.1 cm, W = 1.0 cm, C_{dl} = 50 μF/cm^2, C_E = 7.17×10^{-5} μF/cm^2, L_s = 1.255×10^{-9} H/m.

SEP 08 1986

DL/1113/86/2

TECHNICAL REPORT DISTRIBUTION LIST, GEN

	No. Copies
Office of Naval Research Attn: Code 1113 800 N. Quincy Street Arlington, Virginia 22217-5000	2
Dr. Bernard Douda Naval Weapons Support Center Code 50C Crane, Indiana 47522-5050	1
Naval Civil Engineering Laboratory Attn: Dr. R. W. Drisko, Code L52 Port Hueneme, California 93401	1
Defense Technical Information Center Building 5, Cameron Station Alexandria, Virginia 22314	12 high quality
DTNSRDC Attn: Dr. H. Singerman Applied Chemistry Division Annapolis, Maryland 21401	1
Dr. William Tolles Superintendent Chemistry Division, Code 6100 Naval Research Laboratory Washington, D.C. 20375-5000	1
Dr. David Young Code 334 NORDA NSTL, Mississippi 39529	1
Naval Weapons Center Attn: Dr. Ron Atkins Chemistry Division China Lake, California 93555	1
Scientific Advisor Commandant of the Marine Corps Code RD-1 Washington, D.C. 20380	1
U.S. Army Research Office Attn: CRD-AA-IP P.O. Box 12211 Research Triangle Park, NC 27709	1
Mr. John Boyle Materials Branch Naval Ship Engineering Center Philadelphia, Pennsylvania 19112	1
Naval Ocean Systems Center Attn: Dr. S. Yamamoto Marine Sciences Division San Diego, California 91232	1

Ant 1972

DL/1113/86/2

ABSTRACTS DISTRIBUTION LIST, 056/625/629

Dr. J. E. Jensen
Hughes Research Laboratory
3011 Malibu Canyon Road
Malibu, California 90265

Dr. J. H. Weaver
Department of Chemical Engineering
and Materials Science
University of Minnesota
Minneapolis, Minnesota 55455

Dr. A. Reisman
Microelectronics Center of North Carolina
Research Triangle Park, North Carolina
27709

Dr. M. Grunze
Laboratory for Surface Science and
Technology
University of Maine
Orono, Maine 04469

Dr. J. Butler
Naval Research Laboratory
Code 6115
Washington D.C. 20375-5000

Dr. L. Interante
Chemistry Department
Rensselaer Polytechnic Institute
Troy, New York 12181

Dr. Irvin Heard
Chemistry and Physics Department
Lincoln University
Lincoln University, Pennsylvania 19352

Dr. K.J. Klaubunde
Department of Chemistry
Kansas State University
Manhattan, Kansas 66506

Dr. C. B. Harris
Department of Chemistry
University of California
Berkeley, California 94720

Dr. F. Kutzler
Department of Chemistry
Box 5055
Tennessee Technological University
Cookesville, Tennessee 38501

Dr. D. DiLella
Chemistry Department
George Washington University
Washington D.C. 20052

Dr. R. Reeves
Chemistry Department
Renssaeler Polytechnic Institute
Troy, New York 12181

Dr. Steven M. George
Stanford University
Department of Chemistry
Stanford, CA 94305

Dr. Mark Johnson
Yale University
Department of Chemistry
New Haven, CT 06511-8118

Dr. W. Knauer
Hughes Research Laboratory
3011 Malibu Canyon Road
Malibu, California 90265

/4ct 1 1'2

DL/1113/86/2

ABSTRACTS DISTRIBUTION LIST, 056/625/629

Dr. G. A. Somorjai
Department of Chemistry
University of California
Berkeley, California 94720

Dr. J. Murday
Naval Research Laboratory
Code 6170
Washington, D.C. 20375-5000

Dr. J. B. Hudson
Materials Division
Rensselaer Polytechnic Institute
Troy, New York 12181

Dr. Theodore E. Madey
Surface Chemistry Section
Department of Commerce
National Bureau of Standards
Washington, D.C. 20234

Dr. J. E. Demuth
IBM Corporation
Thomas J. Watson Research Center
P.O. Box 218
Yorktown Heights, New York 10598

Dr. M. G. Lagally
Department of Metallurgical
and Mining Engineering
University of Wisconsin
Madison, Wisconsin 53706

Dr. R. P. Van Duyne
Chemistry Department
Northwestern University
Evanston, Illinois 60637

Dr. J. M. White
Department of Chemistry
University of Texas
Austin, Texas 78712

Dr. D. E. Harrison
Department of Physics
Naval Postgraduate School
Monterey, California 93940

Dr. R. L. Park
Director, Center of Materials
Research
University of Maryland
College Park, Maryland 20742

Dr. W. T. Peria
Electrical Engineering Department
University of Minnesota
Minneapolis, Minnesota 55455

Dr. Keith H. Johnson
Department of Metallurgy and
Materials Science
Massachusetts Institute of Technology
Cambridge, Massachusetts 02139

Dr. S. Sibener
Department of Chemistry
James Franck Institute
5640 Ellis Avenue
Chicago, Illinois 60637

Dr. Arnold Green
Quantum Surface Dynamics Branch
Code 3817
Naval Weapons Center
China Lake, California 93555

Dr. A. Wold
Department of Chemistry
Brown University
Providence, Rhode Island 02912

Dr. S. L. Bernasek
Department of Chemistry
Princeton University
Princeton, New Jersey 08544

Dr. W. Kohn
Department of Physics
University of California, San Diego
La Jolla, California 92037

DL/1113/86/2

ABSTRACTS DISTRIBUTION LIST, 056/625/629

Dr. F. Carter
Code 6170
Naval Research Laboratory
Washington, D.C. 20375-5000

Dr. Richard Colton
Code 6170
Naval Research Laboratory
Washington, D.C. 20375-5000

Dr. Dan Pierce
National Bureau of Standards
Optical Physics Division
Washington, D.C. 20234

Dr. R. Stanley Williams
Department of Chemistry
University of California
Los Angeles, California 90024

Dr. R. P. Messmer
Materials Characterization Lab.
General Electric Company
Schenectady, New York 22217

Dr. Robert Gomer
Department of Chemistry
James Franck Institute
5640 Ellis Avenue
Chicago, Illinois 60637

Dr. Ronald Lee
R301
Naval Surface Weapons Center
White Oak
Silver Spring, Maryland 20910

Dr. Paul Schoen
Code 6190
Naval Research Laboratory
Washington, D.C. 20375-5000

Dr. John T. Yates
Department of Chemistry
University of Pittsburgh
Pittsburgh, Pennsylvania 15260

Dr. Richard Greene
Code 5230
Naval Research Laboratory
Washington, D.C. 20375-5000

Dr. L. Kesmodel
Department of Physics
Indiana University
Bloomington, Indiana 47403

Dr. K. C. Janda
University of Pittsburg
Chemistry Building
Pittsburg, PA 15260

Dr. E. A. Irene
Department of Chemistry
University of North Carolina
Chapel Hill, North Carolina 27514

Dr. Adam Heller
Bell Laboratories
Murray Hill, New Jersey 07974

Dr. Martin Fleischmann
Department of Chemistry
University of Southampton
Southampton 509 5NH
UNITED KINGDOM

Dr. H. Tachikawa
Chemistry Department
Jackson State University
Jackson, Mississippi 39217

Dr. John W. Wilkins
Cornell University
Laboratory of Atomic and
Solid State Physics
Ithaca, New York 14853

DL/1113/86/2

ABSTRACTS DISTRIBUTION LIST, 056/625/629

Dr. R. G. Wallis
Department of Physics
University of California
Irvine, California 92664

Dr. D. Ramaker
Chemistry Department
George Washington University
Washington, D.C. 20052

Dr. J. C. Hemminger
Chemistry Department
University of California
Irvine, California 92717

Dr. T. F. George
Chemistry Department
University of Rochester
Rochester, New York 14627

Dr. G. Rubloff
IBM
Thomas J. Watson Research Center
P.O. Box 218
Yorktown Heights, New York 10598

Dr. Horia Metiu
Chemistry Department
University of California
Santa Barbara, California 93106

Dr. W. Goddard
Department of Chemistry and Chemical Engineering
California Institute of Technology
Pasadena, California 91125

Dr. P. Hansma
Department of Physics
University of California
Santa Barbara, California 93106

Dr. J. Baldeschwieler
Department of Chemistry and Chemical Engineering
California Institute of Technology
Pasadena, California 91125

Dr. J. T. Keiser
Department of Chemistry
University of Richmond
Richmond, Virginia 23173

Dr. R. W. Plummer
Department of Physics
University of Pennsylvania
Philadelphia, Pennsylvania 19104

Dr. E. Yeager
Department of Chemistry
Case Western Reserve University
Cleveland, Ohio 41106

Dr. N. Winograd
Department of Chemistry
Pennsylvania State University
University Park, Pennsylvania 16802

Dr. Roald Hoffmann
Department of Chemistry
Cornell University
Ithaca, New York 14853

Dr. A. Steckl
Department of Electrical and Systems Engineering
Rensselaer Polytechnic Institute
Troy, NewYork 12181

Dr. G.H. Morrison
Department of Chemistry
Cornell University
Ithaca, New York 14853

4k pT 171L

DL/1113/86/2

ABSTRACTS DISTRIBUTION LIST, 359/627

Dr. Paul Delahay
Department of Chemistry
New York University
New York, New York 10003

Dr. J. Driscoll
Lockheed Palo Alto Research
Laboratory
3251 Hanover Street
Palo Alto, California 94304

Dr. D. N. Bennion
Department of Chemical Engineering
Brigham Young University
Provo, Utah 84602

Dr. R. A. Marcus
Department of Chemistry
California Institute of Technology
Pasadena, California 91125

Dr. J. J. Auborn
Bell Laboratories
Murray Hill, New Jersey 07974

Dr. Joseph Singer, Code 302-1
NASA-Lewis
21000 Brookpark Road
Cleveland, Ohio 44135

Dr. P. P. Schmidt
Department of Chemistry
Oakland University
Rochester, Michigan 48063

Dr. Roger Belt
Litton Industries Inc.
Airtron Division
Morris Plains, NJ 07950

Dr. Ulrich Stimming
Department of Chemical Engineering
Columbia University
New York, NY 10027

Dr. Manfred Breiter
Institut fur Technische Elektrochemie
Technischen Universitat Wien
9 Getreidemarkt, 1160 Wien
AUSTRIA

~~Dr. E. Yeager~~
~~Department of Chemistry~~
~~Case Western Reserve University~~
~~Cleveland, Ohio 44106~~

Dr. C. E. Mueller
The Electrochemistry Branch
Naval Surface Weapons Center
White Oak Laboratory
Silver Spring, Maryland 20910

Dr. Sam Perone
Chemistry & Materials
Science Department
Lawrence Livermore National Laboratory
Livermore, California 94550

Dr. Royce W. Murray
Department of Chemistry
University of North Carolina
Chapel Hill, North Carolina 27514

Dr. Adam Heller
Bell Laboratories
Murray Hill, New Jersey 07974

Dr. A. B. Ellis
Chemistry Department
University of Wisconsin
Madison, Wisconsin 53706

Dr. Steven Greenbaum
Department of Physics and Astronomy
Hunter College
695 Park Ave.
New York, NY 10021

-Hpt 1986

DL/1113/86/2

ABSTRACTS DISTRIBUTION LIST, 359/627

Dr. M. Wrighton
Chemistry Department
Massachusetts Institute
of Technology
Cambridge, Massachusetts 02139

Dr. B. Stanley Pons
Department of Chemistry
University of Utah
Salt Lake City, Utah 84112

Donald E. Mains
Naval Weapons Support Center
Electrochemical Power Sources Division
Crane, Indiana 47522

S. Ruby
DOE (STOR)
Room 5E036 Forrestal Bldg., CE-14
Washington, D.C. 20595

Dr. A. J. Bard
Department of Chemistry
University of Texas
Austin, Texas 78712

Dr. Janet Osteryoung
Department of Chemistry
State University of New York
Buffalo, New York 14214

Dr. Donald W. Ernst
Naval Surface Weapons Center
Code R-33
White Oak Laboratory
Silver Spring, Maryland 20910

Mr. James R. Moden
Naval Underwater Systems Center
Code 3632
Newport, Rhode Island 02840

Dr. Bernard Spielvogel
U.S. Army Research Office
P.O. Box 12211
Research Triangle Park, NC 27709

Dr. Aaron Fletcher
Naval Weapons Center
Code 3852
China Lake, California 93555

Dr. Michael J. Weaver
Department of Chemistry
Purdue University
West Lafayette, Indiana 47907

Dr. R. David Rauh
EIC Laboratories, Inc.
Norwood, Massachusetts 02062

Dr. Aaron Wold
Department of Chemistry
Brown University
Providence, Rhode Island 02192

Dr. Martin Fleischmann
Department of Chemistry
University of Southampton
Southampton SO9 5NH UNITED KINGDOM

Dr. R. A. Osteryoung
Department of Chemistry
State University of New York
Buffalo, New York 14214

Dr. John Wilkes
Air Force Office of Scientific
Research
Bolling AFB
Washington, D.C. 20332

Dr. D. Rolison
Naval Research Laboratory
Code 6171
Washington, D.C. 20375-5000

Dr. D. F. Shriver
Department of Chemistry
Northwestern University
Evanston, Illinois 60201

Dr. Edward M. Eyring
Department of Chemistry
University of Utah
Salt Lake City, UT 84112

Dr. M. M. Nicholson
Electronics Research Center
Rockwell International
3370 Miraloma Avenue
Anaheim, California

DL/1113/86/2

ABSTRACTS DISTRIBUTION LIST, 359/627

Dr. Hector D. Abruna
Department of Chemistry
Cornell University
Ithaca, New York 14853

Dr. A. B. P. Lever
Chemistry Department
York University
Downsview, Ontario M3J1P3

Dr. Stanislaw Szpak
Naval Ocean Systems Center
Code 633, Bayside
San Diego, California 95152

Dr. Gregory Farrington
Department of Materials Science
and Engineering
University of Pennsylvania
Philadelphia, Pennsylvania 19104

M. L. Robertson
Manager, Electrochemical
and Power Sources Division
Naval Weapons Support Center
Crane, Indiana 47522

Dr. T. Marks
Department of Chemistry
Northwestern University
Evanston, Illinois 60201

Dr. Micha Tomkiewicz
Department of Physics
Brooklyn College
Brooklyn, New York 11210

Dr. Lesser Blum
Department of Physics
University of Puerto Rico
Rio Piedras, Puerto Rico 00931

Dr. Joseph Gordon, II
IBM Corporation
5600 Cottle Road
San Jose, California 95193

Dr. Nathan Lewis
Department of Chemistry
Stanford University
Stanford, California 94305

Dr. D. H. Whitmore
Department of Materials Science
Northwestern University
Evanston, Illinois 60201

Dr. Alan Bewick
Department of Chemistry
The University of Southampton
Southampton, SO9 5NH UNITED KINGDOM

Dr. E. Anderson
NAVSEA-56Z33 NC #4
541 Jefferson Davis Highway
Arlington, VA

Dr. Bruce Dunn
Department of Engineering &
Applied Science
University of California
Los Angeles, California 90024

Dr. Elton Cairns
Energy & Environment Division
Lawrence Berkeley Laboratory
University of California
Berkeley, California 94720

Dr. Richard Pollard
Department of Chemical Engineering
University of Houston
Houston, Texas 77004

Dr. M. Philpott
IBM Corporation
5600 Cottle Road
San Jose, California 95193

Dr. Donald Sandstrom
Boeing Aerospace Co.
P.O. Box 3999
Seattle, Washington 98124

Dr. Carl Kannewurf
Department of Electrical Engineering
and Computer Science
Northwestern University
Evanston, Illinois 60201

Dr. Joel Harris
Department of Chemistry
University of Utah
Salt Lake City, Utah 84112

4 ept 1/1?

DL/1113/86/2

ABSTRACTS DISTRIBUTION LIST, 359/627

Dr. Robert Somoano
Jet Propulsion Laboratory
California Institute of Technology
Pasadena, California 91103

Dr. Johann A. Joebstl
USA Mobility Equipment R&D Command
DRDME-EC
Fort Belvoir, Virginia 22060

Dr. Judith H. Ambrus
NASA Headquarters
M.S. RTS-6
Washington, D.C. 20546

Dr. Albert R. Landgrebe
U.S. Department of Energy
M.S. 6B025 Forrestal Building
Washington, D.C. 20595

Dr. J. J. Brophy
Department of Physics
University of Utah
Salt Lake City, Utah 84112

Dr. Charles Martin
Department of Chemistry
Texas A&M University
College Station, Texas 77843

Dr. H. Tachikawa
Department of Chemistry
Jackson State University
Jackson, Mississippi 39217

Dr. Farrell Lytle
Boeing Engineering and
Construction Engineers
P.O. Box 3707
Seattle, Washington 98124

Dr. Robert Gotscholl
U.S. Department of Energy
MS G-226
Washington, D.C. 20545

Dr. Edward Fletcher
Department of Mechanical Engineering
University of Minnesota
Minneapolis, Minnesota 55455

Dr. John Fontanella
Department of Physics
U.S. Naval Academy
Annapolis, Maryland 21402

Dr. Martha Greenblatt
Department of Chemistry
Rutgers University
New Brunswick, New Jersey 08903

Dr. John Wasson
Syntheco, Inc.
Rte 6 - Industrial Pike Road
Gastonia, North Carolina 28052

Dr. Walter Roth
Department of Physics
State University of New York
Albany, New York 12222

Dr. Anthony Sammells
Eltron Research Inc.
4260 Westbrook Drive, Suite 111
Aurora, Illinois 60505

Dr. C. A. Angell
Department of Chemistry
Purdue University
West Lafayette, Indiana 47907

Dr. Thomas Davis
Polymer Science and Standards
Division
National Bureau of Standards
Washington, D.C. 20234

Sept 1986

ABSTRACTS DISTRIBUTION LIST, 359/627

Dr. John Owen
Department of Chemistry and
Applied Chemistry
University of Salford
Salford M5 4WT ENGLAND

Dr. Boone Owens
Department of Chemical Engineering
and Materials Science
University of Minnesota
Minneapolis, Minnesota 55455

Dr. Menahem Anderman
W.R. Grace & Co.
Columbia, MD 20144

Dr. J. O. Thomas
University of Uppsala
Institute of Chemistry
Box 531
S-751 21 Uppsala, Sweden

Dr. O. Stafsudd
Department of Electrical Engineering
University of California
Los Angeles, California 90024

ABSTRACTS DISTRIBUTION LIST, SDIO/IST

Dr. Robert A. Osteryoung
Department of Chemistry
State University of New York
Buffalo, NY 14214

Dr. Douglas N. Bennion
Department of Chemical Engineering
Brigham Young University
Provo, UT 84602

Dr. Stanley Pons
Department of Chemistry
University of Utah
Salt Lake City, UT 84112

Dr. Joseph R. Driscoll
Lockheed Missile and Space Co.
Palo Alto Research Labs
Palo Alto, CA 94304

Dr. R. David Rauh
EIC Labs Inc.
111 Downey St.
Norwood, MA 02062

Dr. Neill Weber
Ceramatec, Inc.
163 West 1700 South
Salt Lake City, UT 84115

Dr. Subhash C. Narang
SRI International
333 Ravenswood Ave.
Menlo Park, CA 94025

Dr. J. Paul Pemsler
Castle Technology Corporation
52 Dragon Ct.
Woburn, MA 01801

Dr. Donald M. Schleich
Department of Chemistry
Polytechnic Institute of New York
333 Jay St.
Brooklyn, NY 11201

Dr. Stan Szpak
Code 633
Naval Ocean Systems Center
San Diego, CA 92152-5000

Dr. George Blomgren
Battery Products Division
Union Carbide Corporation
25225 Detroit Rd.
Westlake, OH 44145

Dr. Earnest Yeager
Case Center for Electrochemical Science
Case Western Reserve University
Cleveland, OH 44106

Dr. Aaron N. Fletcher
Code 3852
Naval Weapons Center
China Lake, CA 93555

Dr. Michael J. Weaver
Department of Chemistry
Purdue University
West Lafayette, IN 47907

END
9-87
DTIC